

The effect of frost weathering at the dinosaur tracksite in Seoyu-ri, Hwasun, Korea

Jihwan Park^{1,2} · Hyeong-Dong Park^{1,2}

Received: 15 June 2016 / Accepted: 31 October 2016 / Published online: 8 November 2016
© Springer-Verlag Berlin Heidelberg 2016

Abstract Cultural monuments and geological heritage sites composed of natural stone are severely affected by frost weathering in cold regions or during the winter season in mid-altitude regions. The effect also occurs at the dinosaur tracksite in Seoyu-ri, Hwasun, Korea, which is not sheltered. To assess the influence of frost weathering on the tracksite, freeze–thaw experiments were carried out in the laboratory up to 100 cycles, simulating geological and meteorological conditions of the site. The variation on physical properties were measured at a core scale as weathering progressed. The decreases in dry weight, P- and S-wave velocity, and elastic modulus, and the increase in absorption rate and Poisson’s ratio showed the physical deterioration of the specimens. The microstructural properties were also measured using micro-computed tomography (micro-CT) images as weathering progressed. The variation on porosity (especially open porosity), pore size distribution, local thickness, and crack orientation showed the propagation and expansion of the pores and microcracks in rock specimens at a pore scale. Because every measurement was performed using non-destructive methods, the variation on the same specimens can be analyzed continuously. The results showed that frost weathering can cause damage to the tracksites. This research, therefore, suggests the construction of a shelter to maintain the temperature of the tracksite and to prevent groundwater seepage. This research can be applied to assess the effects

of frost weathering at other cultural stone heritage or geological heritage sites.

Keywords Frost weathering · Dinosaur tracksite · Geological heritage · Micro-CT · Porosity · Microcrack

Introduction

Cultural monuments and geological heritage sites composed of natural stone, particularly sandstone, can be severely affected by weathering processes (Grassegger 1999). The three types of rock weathering include physical weathering, which causes mechanical disintegration and breaks down rocks into small particles without chemical changes; chemical weathering, which changes the composition of rocks by the action of chemical agents; and biological weathering caused by living things such as animals, plants, and microorganisms. Generally, these types of weathering processes occur together. The physical properties of rock specimens are deteriorated as weathering progresses (Tugrul and Zarif 2000). In cold regions or during the winter season in mid-altitude regions, physical weathering caused by freezing and thawing occurs frequently because the temperature oscillates at about 0 °C.

In the present study, the effect of frost weathering occurring at the dinosaur tracksite in Seoyu-ri, Hwasun, is considered. Because the site is in Korea, which is located at mid-latitude, the temperature variation is conducive to frost weathering. In addition, this site is not sheltered, which has hastened physical weathering such as frost weathering caused by temperature changes.

A significant amount of dinosaur trace fossils has been found in the Korean Peninsula. After Yang (1982) discovered the footprints of a dinosaur at Goseong-gun,

✉ Hyeong-Dong Park
hpark@snu.ac.kr

¹ Department of Energy Systems Engineering, Seoul National University, Gwanak-ro 1, Gwanak-gu, Seoul 08826, Korea

² Research Institute of Energy and Resources, Seoul National University, Gwanak-ro 1, Gwanak-gu, Seoul 08826, Korea

Gyeongsangnam-do, Korea, many investigators have studied and reported the existence of dinosaur trace fossils throughout the country (Houck and Lockley 2006; Minter et al. 2012; Kim and Lockley 2012; Paik et al. 2006). Thus far, 11 sites have been designated as natural monuments in Korea (Table 1). The United Nations Educational, Scientific and Cultural Organization (UNESCO) has released a tentative list of fossilized dinosaur sites throughout the South Korean seacoast. Based on their high geological and cultural value, these sites include the tracksite of dinosaurs, pterosaurs, and birds in Uhang-ri, Haenam (no. 394), the tracksite of dinosaurs and birds in Deongmyeong-ri, Goseon (no. 411), the fossil site of dinosaur eggs in Bibong-ri, Boseong (no. 418), the dinosaur tracksite and sedimentary rocks in Nangdo-ri, Yeosu (no. 434), and the dinosaur tracksite in Seoyu-ri, Hwasun (no. 487).

Among these tracksites, the dinosaur tracksite in Seoyu-ri, Hwasun, is of high importance. Since its discovery in 1999, this site has been investigated continuously by many researchers. More than 1340 dinosaur footprints and trackways have been discovered, and sedimentary structures such as sun cracks, ripple marks, petrified wood, and plant fossils have been reported (Lockley et al. 2012). Huh et al. (2006) classified the types of dinosaur footprints and estimated their sizes and walking speed. Kim and Huh (2010) analyzed the stride length and running speed of the dinosaurs. However, such research tends to focus on the geological and paleobiological implications rather than rock weathering at the dinosaur tracksite.

When the temperature of water trapped in pores, cracks, and fissures within rocks drops below the freezing point, the water freezes to ice. Because the ice occupies 9.05% greater volume, it exerts pressure on the surrounding rock surface (Shen et al. 2015). Therefore, repeated cycles of freezing and thawing can deteriorate rock. Frost weathering has long been discussed. Many researchers have simulated frost weathering by using

laboratory tests that focus on the physical properties of rocks. Potts (1970) performed 200 cycles of freezing and thawing on sedimentary rocks such as sandstones, mudstones, shales, and conglomerates under temperature variations of -8 to $+8$ °C and from -30 to $+15$ °C and measured the weight loss as the weathering progressed. Masuoka (1990) performed up to 1000 freezing and thawing cycles and analyzed the cubic shape of 28 sedimentary rocks, 18 metamorphic rocks, and 1 igneous rock under temperatures ranging from -20 to $+20$ °C by measuring the variation of dry weight, P-wave velocity, porosity, and other parameters. Altindig et al. (2004) performed 55 cycles of freezing and thawing on ignimbrite under temperatures ranging from -20 to $+20$ °C and measured the changes in uniaxial compressive strength, point load strength, P-wave velocity, and porosity. Thomachot and Matsuoka (2007) investigated the dilation of sandstones, molasses, and volcanic tuff and brick from various stone monuments under a temperature range of -8 to $+5$ °C. Other studies have considered the microstructural properties of rocks by using X-ray computed tomography (CT). Ruiz de Argandoña et al. (1999) performed 12 freeze–thaw cycles on dolomite rock specimens and observed the evolution of void structures based on 50 slices of CT images. De Kock et al. (2015) conducted 84 freeze–thaw cycles on limestone under temperatures ranging from -12 to $+20$ °C. Weight, porosity, capillary coefficient, and elastic wave velocity were measured and X-ray CT images were analyzed as the weathering progressed. Park et al. (2015) performed 150 freezing and thawing cycles from -20 to $+10$ °C on diorite, basalt, and tuff specimens. Physical properties including porosity, P- and S-wave velocities, and dry weight were measured, and scanning electron microscopy (SEM) and X-ray CT images were obtained to analyze the microstructural changes in the specimens.

Table 1 Natural monuments related to dinosaur trace fossils in Korea

Natural monument no.	Name	Location	Designated year
373	Dinosaur tracksite in Jeo-ri, Uiseong	Gyeongsangbuk-do	1993
394	Tracksite of dinosaurs, pterosaurs, and birds in Uhang-ri, Haenam	Jeollanam-do	1998
395	Tracksite of birds and dinosaurs in Gajin-ri, Jinju	Gyeongsangnam-do	1998
411	Tracksite of dinosaurs and birds in Deongmyeong-ri, Goseong	Gyeongsangnam-do	1999
414	Fossil site of dinosaur eggs in Gojeong-ri, Hwaseong	Gyeonggi-do	2000
418	Fossil site of dinosaur eggs in Bibong-ri, Boseong	Jeollanam-do	2000
434	Dinosaur tracksite and sedimentary rocks in Nangdo-ri, Yeosu	Jeollanam-do	2003
474	Dinosaur fossil site on Aduseom Island, Sacheon	Gyeongsangnam	2006
487	Dinosaur tracksite in Seoyu-ri, Hwasun	Jeollanam-do	2007
534	Tracksite of pterosaurs, birds, and dinosaurs in Hotan-dong, Jinju	Gyeongsangnam	2011
548	Tracksite of dinosaurs and pterosaurs in Sanbuk-dong, Gunsan	Jeollabuk-do	2014

The objective of this paper is to investigate the effect of frost weathering on the dinosaur tracksite in Seoyu-ri, Hwasun, Korea. To achieve this aim, the frost weathering conditions of the site were simulated in a laboratory, and the physical and microstructural properties were measured and analyzed as the weathering progressed.

Study area

The dinosaur tracksite of Seoyu-ri, located in northern part of Hwasun County, Jeollanam-do, Korea ($35^{\circ}10'0''\text{N}$, $127^{\circ}05'2''\text{E}$, WGS 84; Fig. 1), was exposed during the process of construction in a quarry inside a hot spring complex in May 1999.

Geological context

The tracksite is situated in the Cretaceous Jangdong Tuff, which consists of tuff breccia, tuffaceous shale, yellow-greenish and yellow-reddish shale and sandstone, and greenish tuff. Jangdong Tuff overlies the Oryeri Formation consisting of a reddish conglomerate, sandstone, and tuff, and the Manweolsan Tuff consisting of gray-greenish fine-grained lapilli tuff. These layers underlie the Jeokbyeok Tuff consisting of fine-grained and coarse-

grained tuff; the Mudeungsan Flow, which is andesitic lava flow; and the Yeonhwari Formation consisting of a reddish conglomerate and reddish light-gray sandstone (Kim and Park 1966). Similar rock types in Korea have been reported to be susceptible to erosion (Lee and Park 2014).

Mineralogical analyses of samples around the site were performed by the X-ray diffraction (XRD) method and polarized light microscopy of thin sections (Fig. 2). Constitutional minerals are albite, quartz, orthoclase, montmorillonite, muscovite, illite, chlorite, and kaolinite. Poorly sorted silt, clay, and sub-angular quartz grains were observed; thin parallel lamination with less than 3-mm thickness was developed.

Engineering geological properties

The dip of the tracksite ranges from 15° to 18° , and the dip direction ranges from N68E to N75E. The area of the site is $34,000\text{ m}^2$. The site is surrounded by two rock slopes: a northern slope with a dip direction of 203° and a dip of 86°SW and a western slope with a dip direction of 300° and a dip of 88°NW (Fig. 3a). Because the two slopes have inclinations of nearly 90° and numerous discontinuities, the risk of rockfall is high. Some fragments of rock produced by rockfall were detected in a field survey (Fig. 3b). These

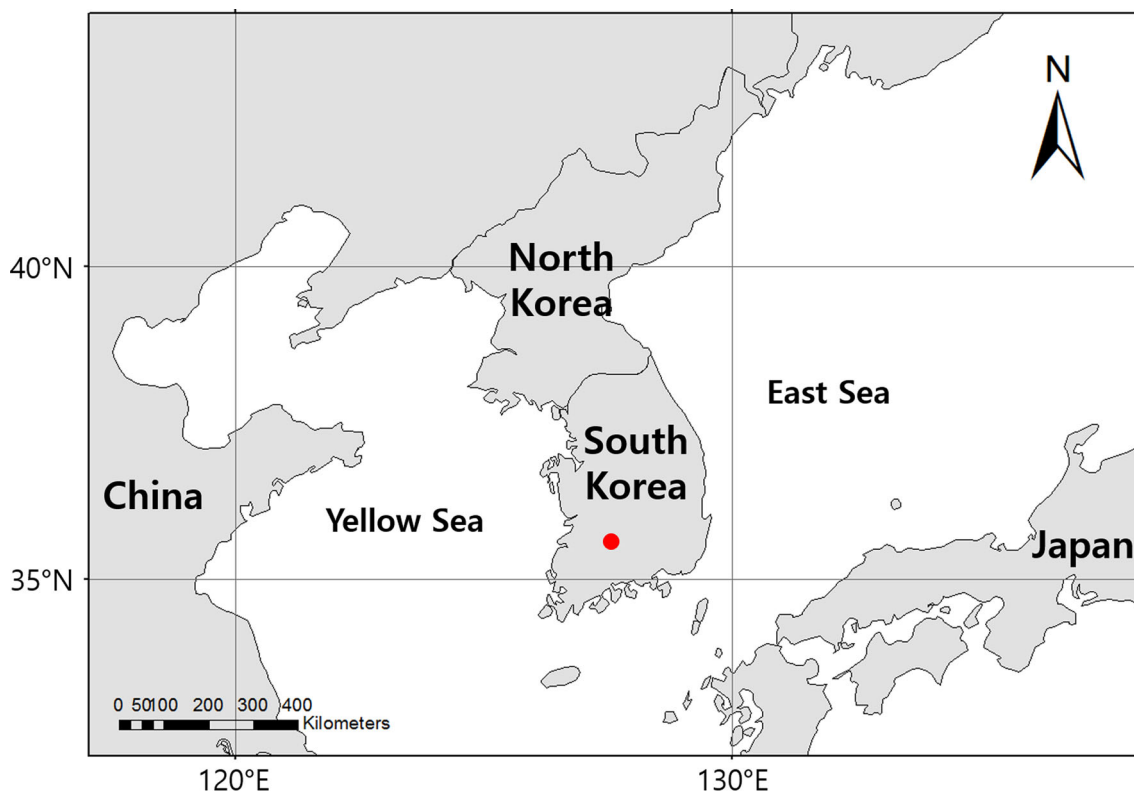


Fig. 1 Location of the dinosaur tracksite in Seoyu-ri, Hwasun County, Jeollanam-do, Korea

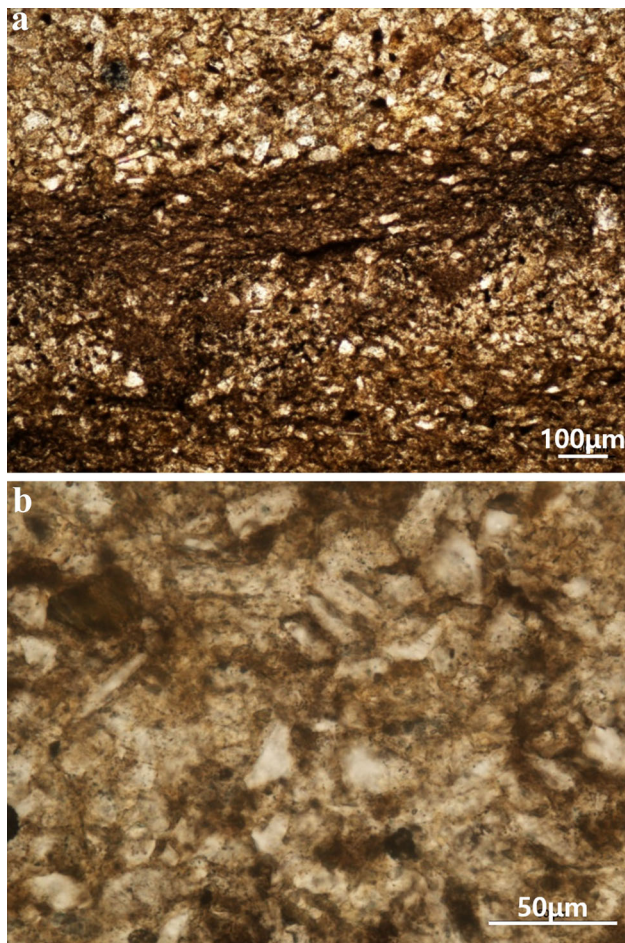


Fig. 2 Thin-section microscope images with crossed polars of the specimen (a) $\times 10$ and (b) $\times 50$ showing thin parallel lamination with poorly sorted silt, clay, and sub-angular quartz grains

rocks can damage the tracksite on the upper plane and threaten the safety of visitors.

Water has consistently flowed on the site owing to improper waterproofing methods (Fig. 3c) and has hastened the rock deterioration caused by physical and chemical weathering. Moreover, frost weathering is severe, particularly during the winter season. Thus, with no further proper conservation plan, severe deterioration of the dinosaur tracksite can occur over time.

Meteorological conditions

Because the site was excavated in May 1999 and has been exposed, temperature observation data provided by the Korea Meteorological Administration from May 1999 to April 2016 were analyzed. The temperature was lowest in January, at 0.8 °C, and highest in August, at 26.3 °C. The minimum and maximum annual temperatures are -18.6 to

-8.6 °C and 32.2 to 37.7 °C, and the average values are 12.5 and 35.1 °C, respectively.

The freezing and thawing conditions of the site are shown in Fig. 4. Overall, 1148 freeze and thaw days were recorded with 269 frozen days; the average was 67.5 freeze and thaw days and 15.8 frozen days per year. The trend shows that over the last 17 years, the annual number of freeze and thaw days increased whereas that of frozen days decreased owing to climate change.

Methodology

In this research, to investigate the effect of frost weathering at the dinosaur tracksite, the environment of the site was simulated in a laboratory. The physical and microstructural properties were measured as the weathering progressed. The specimens used in the frost weathering tests were sampled 500 m from the dinosaur tracksite in the same strata. Because the investigated site is designated as a national heritage site, sampling is restricted. Therefore, the number and sizes of the collected specimens were insufficient for routine analysis of rock mechanics.

The frost weathering tests were conducted on two types of cylindrical specimens. For measuring physical properties, two specimens were cut into lengths of 53.6 to 57.5 mm with a diameter of 37.8 mm. For measuring the microstructural properties, two specimens were cut into lengths of 10.9 to 14.9 mm with a diameter of 9.7 mm to fit the X-ray CT instrument, which has been used as a good tool for analysing the microstructure of rock (Shang et al. 2015).

The specimens were immersed in distilled water for 48 h under atmospheric pressure. The saturated specimens were frozen at -13 °C for 4 h and then thawed at 35 °C in the freezing chamber. The temperature gradient at the increasing or decreasing range was set at 0.8 °C/min to minimize the thermal stress that occurs when the temperature gradient exceeds 2.0 °C/min (Hall 1999). The duration of each freeze–thaw cycle was 10 h (Fig. 5).

Physical deterioration in rock core scale

Up to 100 cycles of frost weathering were simulated in the laboratory to replicate the meteorological conditions of the site. To investigate the variations in the specimens' physical properties, the dry weight, saturated weight, absorption, and P- and S-wave velocities were measured at



Fig. 3 Engineering geological properties of the site. **a** The site is surrounded by northern and western slopes which have a nearly 90° inclination. **b** Rockfall was observed, which can damage the tracksite

and threaten visitors. **c** Groundwater flowed consistently, which can cause deterioration of rock on the site

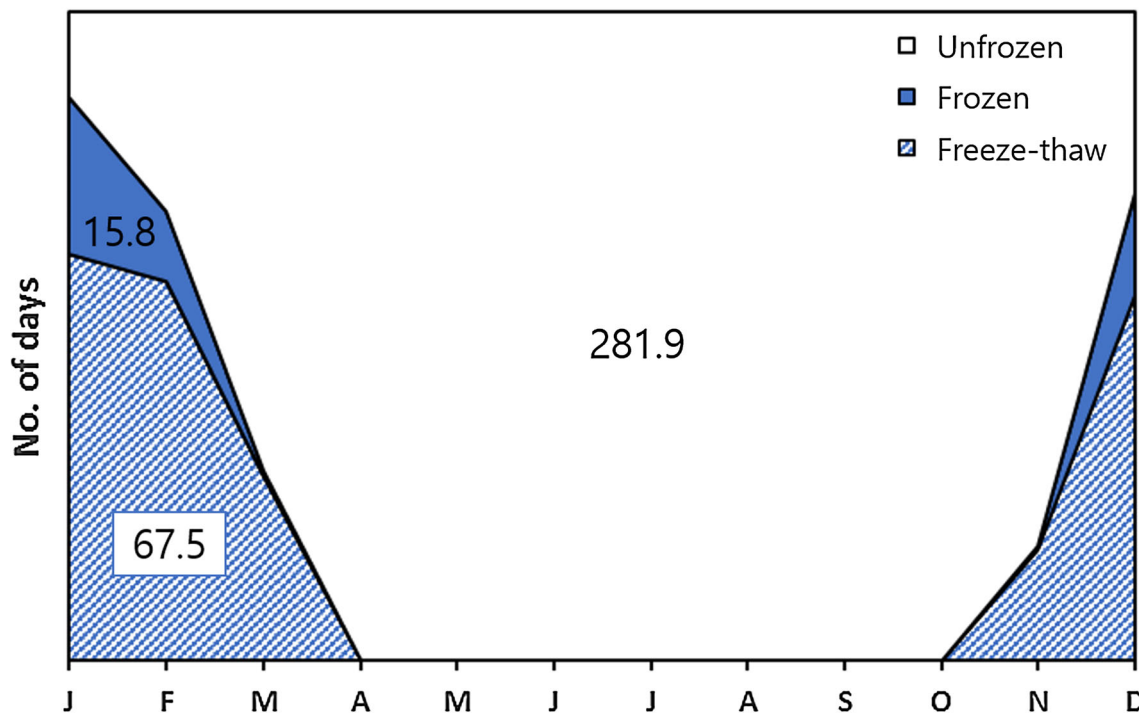


Fig. 4 Freezing and thawing conditions of the site from May 1999 to April 2016. There were, on average, 67.5 freeze–thaw days and 15.8 frozen days per year

intervals of 10 cycles. In this process, the specimens were removed from the freezing chamber, and saturated weight was measured. Then the specimens were dried in an oven at 105 °C for at least 24 h, and the dry weight and P- and S-wave velocities were measured at room temperature

(20 °C). Every measurement was performed according to the method suggested by the International Society for Rock Mechanics (ISRM; Brown 1981). Poisson’s ratio and the elastic modulus were calculated by using the P- and S-wave velocities as

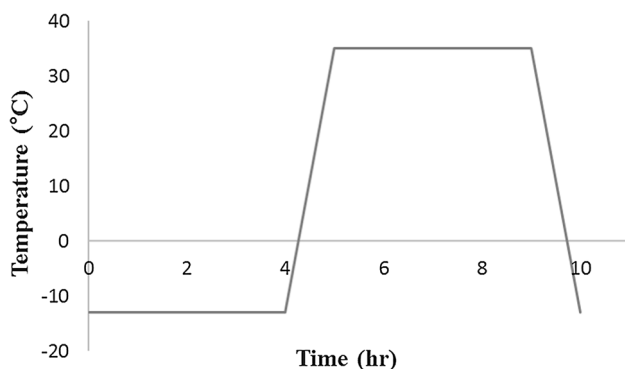


Fig. 5 Temperature cycle used for the artificial frost weathering experiment, which simulated the climatic conditions of the site. One cycle took 10 h and the temperature varied from -13 to 35 °C

$$\sigma = \frac{(z_P/V_S)^2 - 2}{2(V_P/V_S)^2 - 2} \quad (1)$$

$$E = \rho V_S^2 \frac{(V_P/V_S)^2 - 4}{(V_P/V_S)^2 - 1} \quad (2)$$

where σ is Poisson's ratio, E is the elastic modulus, V_P is the P-wave velocity, and V_S is the S-wave velocity. Although the values used in this method can be less accurate than those measured from compressive strength tests, the processes have advantages of simplicity, rapidity, and non-destructivity. Thus, this method is suitable for continuous measurement.

Figure 6a shows the linear decrease in dry weight as frost weathering progressed. The dry weights of both specimens initially were 154.41 and 143.58 g. After 100 cycles of frost weathering, the values were 154.23 and 143.45 g, which show 0.12% and 0.09% decreases, respectively. Figure 6b shows a linear increase in the absorption rate. The absorption rates of both specimens initially were 2.18% and 1.94%. After 100 cycles of frost weathering, the values were 2.38% and 2.10%. Figure 6c shows a linear decrease in P-wave velocity as frost weathering progressed. The P-wave velocities of both specimens were initially 4291 and 4158 m/s. After 100 cycles of weathering, the values were 3859 and 3944 m/s, which show 10.1% and 5.1% decreases, respectively. Figure 6d shows a linear decrease in S-wave velocity as frost weathering progressed. The S-wave velocities of both specimens were initially 2099 and 2063 m/s. After 100 cycles of weathering, the values were 2063 and 1578 m/s, which show 31.5% and 23.5% decreases, respectively. Figure 6e shows a linear increase in Poisson's ratio, which was initially 0.34 for both specimens. After 100 cycles of frost weathering, the absorption rates of both specimens increased to 0.42 and 0.40. Figure 6f shows a linear decrease in the elastic modulus. The elastic modulus values

of both specimens were initially 13.89 and 13.50 GPa. After 100 cycles of frost weathering, the values were 5.75 and 7.08 GPa, which shows decreases of 58.6% and 47.6%, respectively.

Microstructural change at a pore scale

To investigate the variation in microstructural properties of the specimens, X-ray CT images were obtained at increments of 50 cycles. X-ray CT is very powerful non-destructive method used to visualize the interior of rock specimens. Therefore, this method can be used to analyze the changes in the inner structures of rock specimens as weathering progresses without failure of the specimen. In the present research, a SkyScan 1173 high-energy micro-CT was used. The source used was 130 kV with a 60- μ A intensity. The distance between the rock specimen and the X-ray source was 44.212 mm, and that between the camera and the X-ray source was 364.000 mm. We obtained 1200 images with 16-bit intensity, each of which had 1024×1024 pixels. The spatial resolution was 6.04 μ m per pixel. Among them, $800 \times 800 \times 1000$ voxels were selected as the region of interest (ROI). Images were processed with Octopus software 1.1.1.10 (Inside Matters, Belgium).

Variations in porosity, equivalent diameter, local thickness, and crack orientation were analyzed as frost weathering progressed. After binarization to separate the pores and solid parts, porosity can be defined as calculating the proportion of voxels of pores to voxels of ROI. Equivalent diameter is calculated from the pore's equivalent sphere:

$$d_e = \sqrt[3]{\frac{6V}{\pi}} \quad (3)$$

where d_e is the equivalent diameter, and V is the pore volume.

The porosity of sample HS-1 was 3.91% (open and closed porosity were 2.13% and 1.78%, respectively) at the initial state; the value increased to 4.64% (open and closed porosity were 2.90% and 1.74%, respectively) after 50 freeze-thaw cycles; 7.41% (open and closed porosity were 5.58% and 1.83%, respectively) after 100 freeze-thaw cycles. Figure 7a shows the variation in the equivalent diameter of HS-1. The equivalent diameters of the pores were classified into nine groups: 0–50, 50–100, 100–150, 150–200, 200–250, 250–300, 300–350, 350–400 μ m, and more than 400 μ m. The observed pore structures showed that the sizes and numbers of the pores increased as the frost weathering progressed. The total number of pores increased 23% after 100 cycles. Table 2 shows the

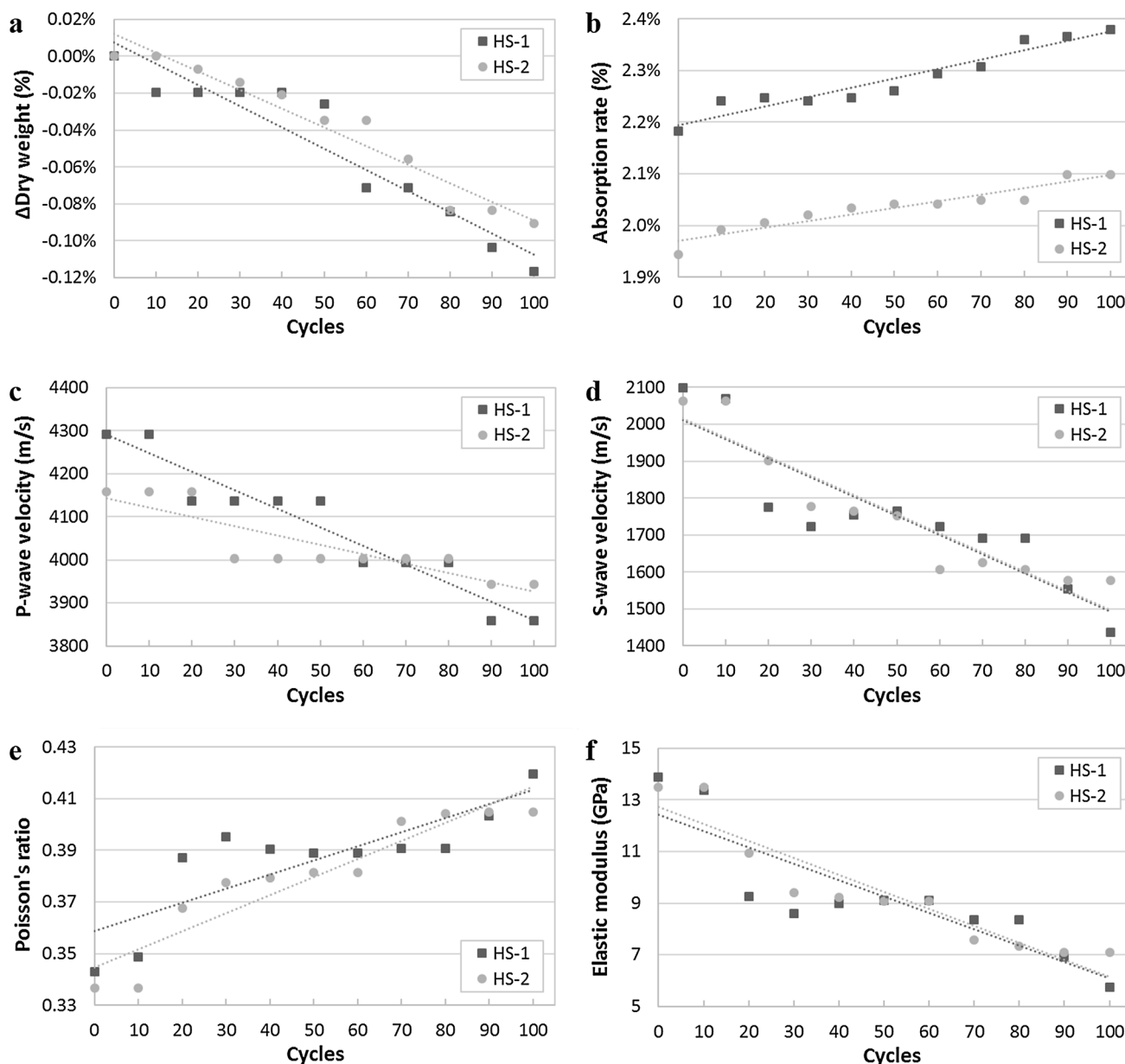


Fig. 6 Variations of physical properties show that the rock specimens were deteriorated as frost weathering progressed: **a** changes in dry weight, **b** absorption rate, **c** P-wave velocity, **d** S-wave velocity, **e** Poisson's ratio and **f** elastic modulus

variation in the number of pores in each group, which increased in most classifications.

The porosity of sample HS-2 was 6.56% (open and closed porosity were 4.38% and 2.17%, respectively) at the initial state; the value increased to 6.98% (open and closed porosity were 4.73% and 2.25%, respectively) after 50 freeze–thaw cycles; 8.15% (open and closed porosity were 5.79% and 2.36%, respectively) after 100 freeze–thaw cycles. Figure 7b shows the variation in the equivalent diameter of HS-2. The equivalent diameters of the pores were classified into the same nine groups as those for HS-1. The observed pore structures showed that the sizes and

numbers of the pores increased as frost weathering progressed. The total number of pores increased 23% after 100 cycles. Table 2 shows the variation in number of pores in each group, which increased in most classifications.

Local thickness is defined as the diameter of the largest inscribed circle that fits inside a pore, which is the shortest local distance between the center of the pore space and the solid part surrounding the pore (Delerue et al. 1999). Local thickness was observed around the skeleton structures of the rock pores in Fig. 8. The local thickness of each pore expanded, and the frequency of each pore increased in Fig. 9. Thickness of less than 3 μm was not detected owing

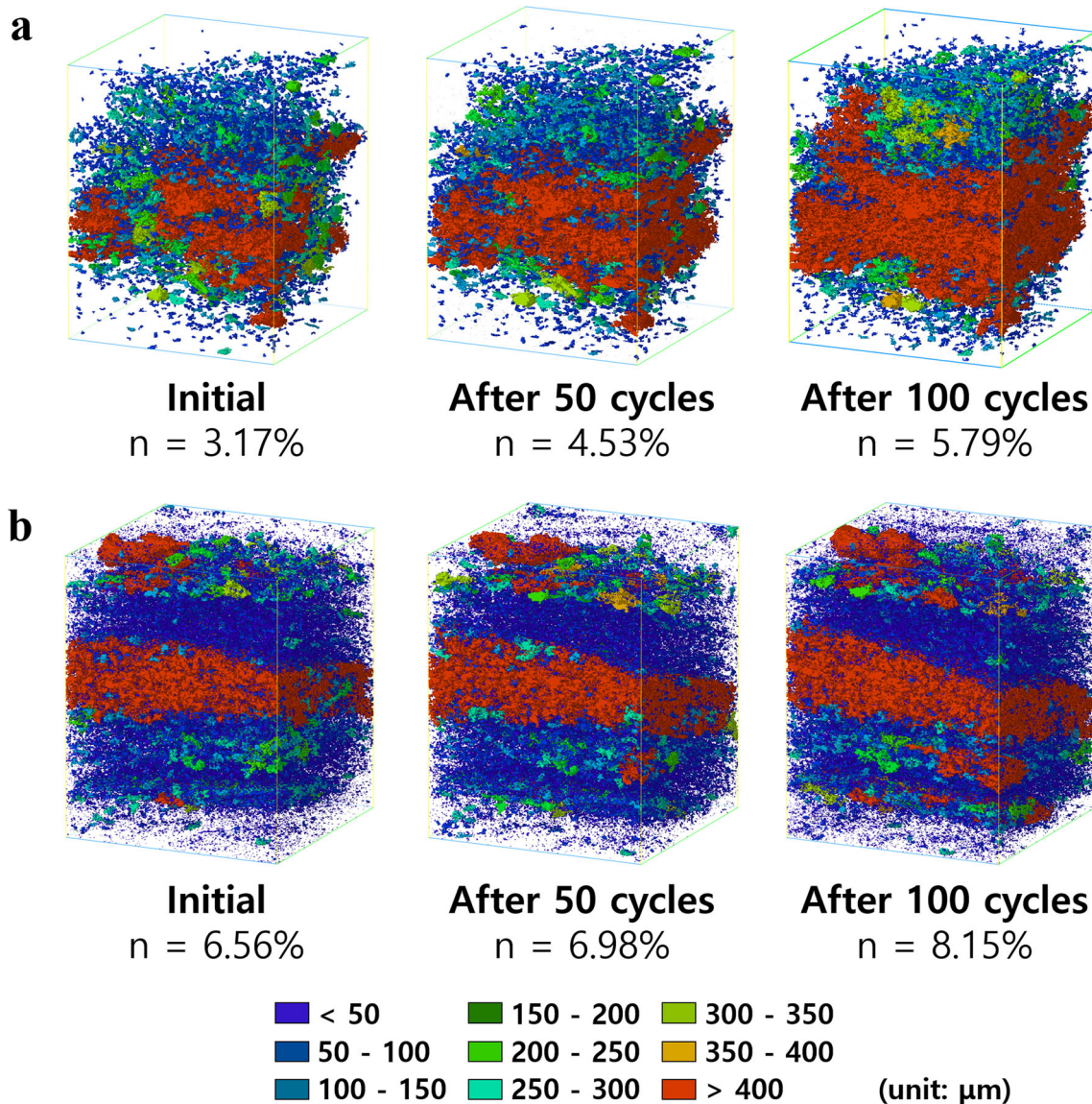


Fig. 7 Variation on equivalent diameter of the specimens at initial state, after 50 freeze–thaw cycles, and after 100 freeze–thaw cycles. The size and number of pores were increased as weathering progresses. **a** Porosity of HS-1 specimen was increased: 3.17% at

the initial state, 4.53% after 50 cycles, and 5.79% after 100 cycles. **b** Porosity of HS-2 specimen was increased: 5.17% at the initial state, 5.65% after 50 cycles, and 6.07% after 100 cycles

to the resolution of the CT image. In both specimens, the number of throats was highest at about $4\ \mu\text{m}$, which is the smallest pore size that can be detected by micro-CT. The trend of distribution did not change as the weathering progressed. The number of throats of specimen HS-1 increased 14–54% and 79–182% after 50 and 100 cycles, respectively. That of specimen HS-2 increased 1–63% and 21–118% after 50 and 100 cycles, respectively.

Crack orientation is defined by analyzing the direction of the skeleton at each point. The direction of the specimen was recorded at the initial state, after 50 cycles, and after 100 cycles. Figure 10 shows the distribution of crack orientations as a rose diagram. The values were classified by 10° . In

specimen HS-1, the orientations were anisotropically distributed at the initial state with the highest at 120° or 300° as 7.09% and the lowest at 30° or 210° as 3.94%. The orientations distributed at 50 freeze–thaw cycles showed the highest at 120° or 300° as 6.89% and the lowest at 50° or 230° as 4.30%. After 100 cycles, the orientations were distributed less anisotropically with the highest at 120° or 300° as 6.67% and the lowest at 50° or 230° as 4.80%. The major orientations remained at 120° or 300° at every cycle. The highest rate of change was 85% at 40° or 220° , and the lowest was 7% at 60° or 240° . In specimen HS-2, the orientations were anisotropically distributed at the initial state with the highest at 150° or 330° as 7.25% and the lowest at

Table 2 Changes on the number of pores of HS-1 in each equivalent diameter group

Equivalent diameter	Frequency			Rate of change (%)
	Initial state	50 cycles	100 cycles	
0–50	19,974	21,065	25,821	+29
50–100	4276	4241	4051	–5
100–150	625	644	571	–9
150–200	194	231	235	+21
200–250	85	105	146	+72
250–300	50	72	75	+50
300–350	21	36	54	+157
350–400	11	21	24	+118
>400	10	24	45	+350
Total	25,246	26,439	31,022	+23

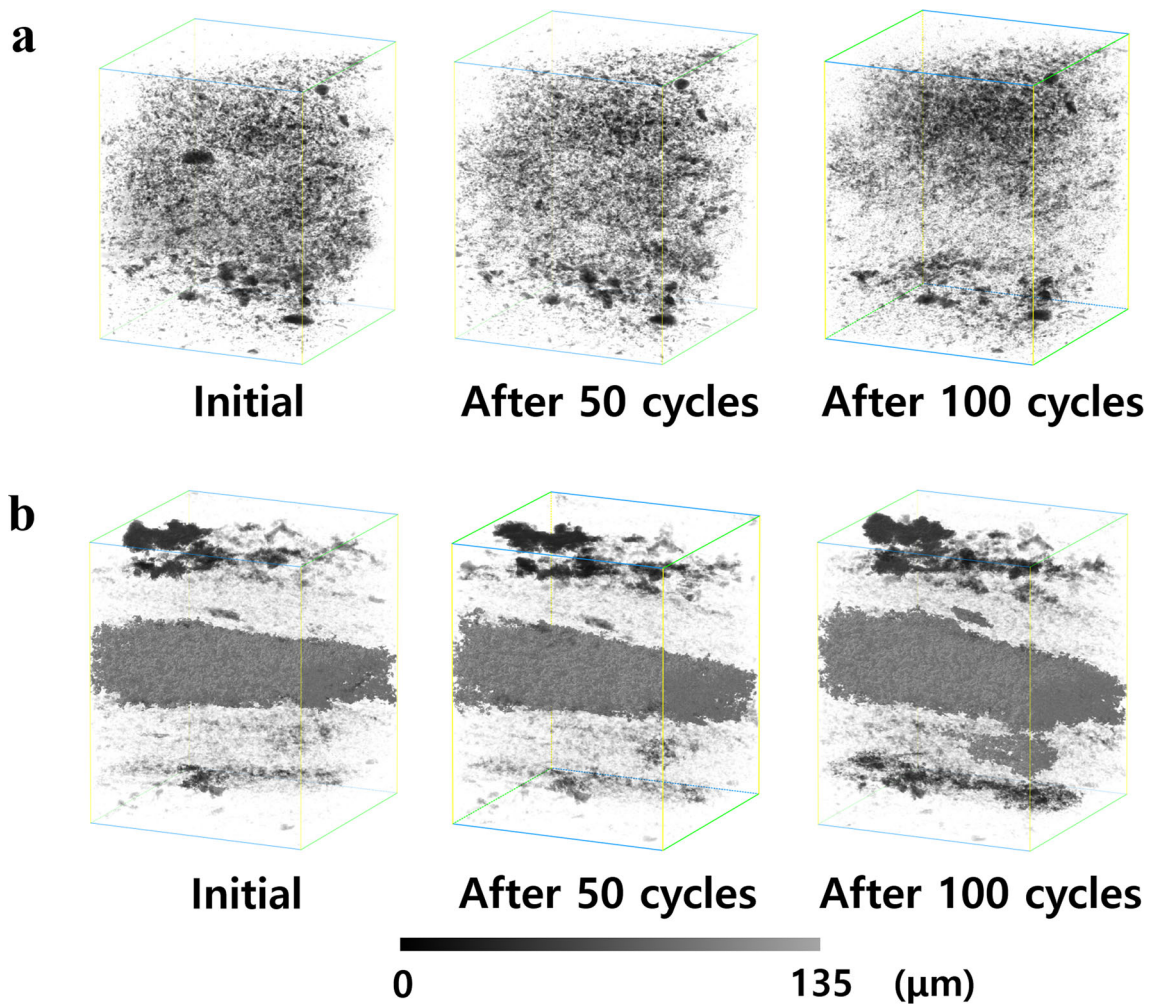


Fig. 8 Variation on local thickness of **a** HS-1 and **b** HS-2 specimens at the initial state, after 50 freeze–thaw cycles, and after 100 freeze–thaw cycles. Local thickness of each pores was expanded and frequency of pores was also increased as weathering progressed

40° or 220° as 3.76%. The distribution patterns were similar at 50 freeze–thaw cycles, with the highest at 150° or 330° as 7.55% and the lowest at 40° or 220° as 3.61%. After 100 cycles, the orientations were distributed less anisotropically

with the highest at 150° or 330° as 6.34% and the lowest at 0° or 180° as 4.69%. The major orientations remained at 150° or 330° at every cycle. The highest rate of change was 85% at 50° or 230°, and the lowest was 77% at 150° or 330°.

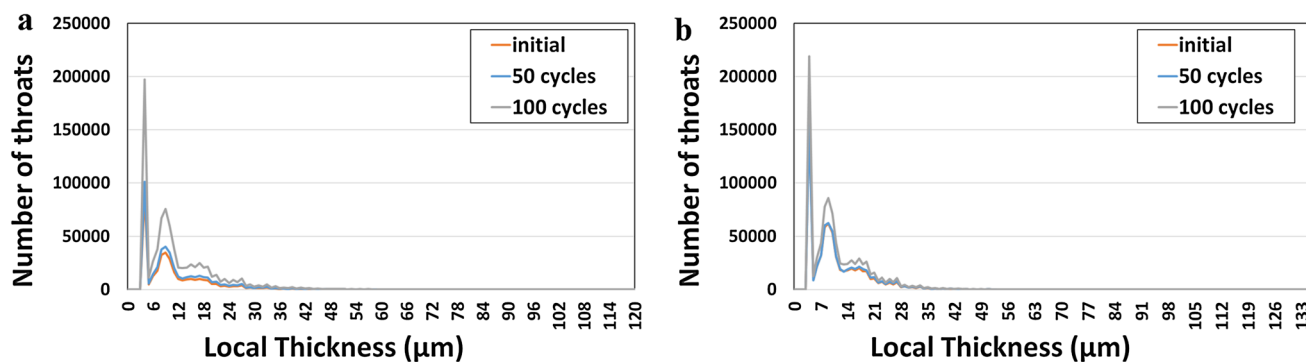


Fig. 9 Variation on local thickness distribution of **a** HS-1 and **b** HS-2. Number of throats were increased in every thickness

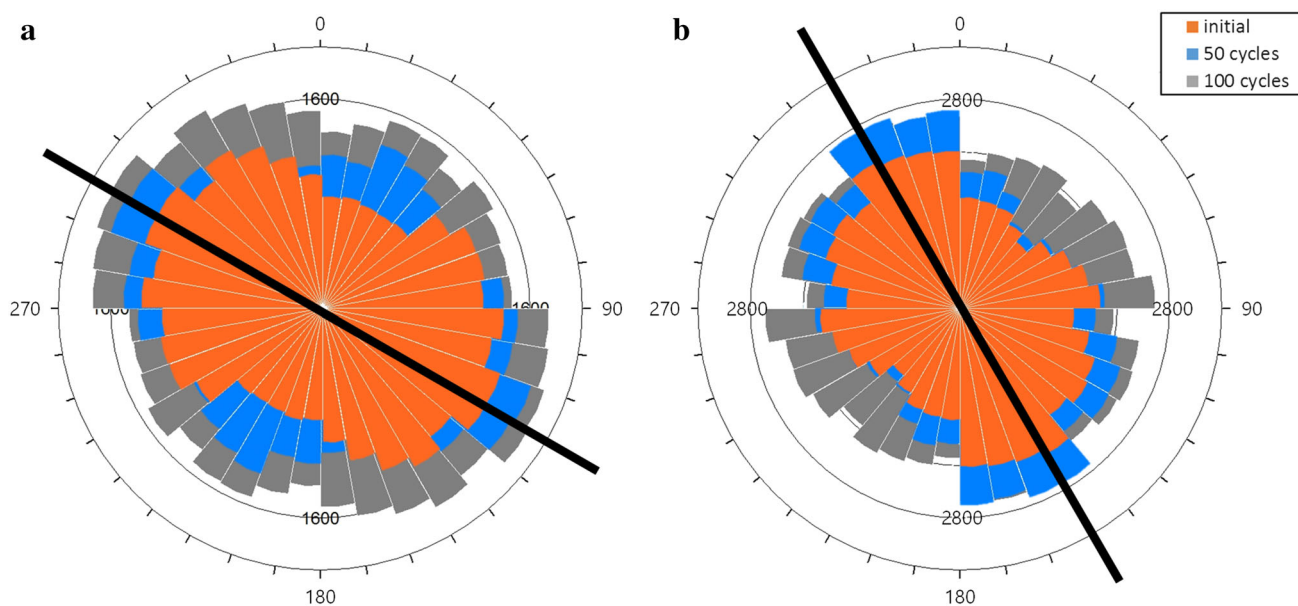


Fig. 10 Variation on crack orientation of the specimen as weathering progressed. The cracks developed in every direction as weathering progressed. The *black line* indicates the major crack orientation, which remained after frost weathering

Discussions

The present study focused on assessing the influence of frost weathering on the dinosaur tracksite in Seoyu-ri. The physical and microstructural properties deteriorated as the frost weathering tests progressed. These results are in close agreement with those of numerous investigations (Martínez-Martínez et al. 2013; Nicholson and Nicholson 2000).

Only non-destructive methods were used to measure the variation of the same specimen without rock failure. The weight (absorption rate) decreased (increased) linearly owing to particle detachment and crack propagation inside the rock specimens. In our recent paper (Park et al. 2015), these phenomena were observed in SEM and CT images of a tuff specimen having similar physical properties as those of the specimens in the present research. The P- and S-wave velocities decreased linearly; that in the latter was significantly greater than that in the former. Because elastic

waves cannot progress through air and thus change direction in crack areas, the wave velocity decreases when the crack density increases. The Poisson's ratio of both specimens was increased linearly, which is in agreement with previous studies comparing Poisson's ratio of weathered and unweathered rock specimens (Saliu and Lawal 2014). This result occurred because unweathered rocks with high Poisson's ratios exhibit more brittle behavior during deformation. The elastic moduli of both specimens decreased about 50% after 100 cycles of frost weathering. Prick (1997) measured the variation in elastic moduli of 10 types of limestones under saturated conditions after one frost weathering experiment; the values decreased 0.19–12.87%.

The porosities of the specimens were increased after freeze–thaw weathering, but there was no significant increase in closed porosity in both specimens. However, open porosities of the specimens were increased 3.45% and

1.41%. The microcracks expanded and propagated because of the development of ice crystals in pores inside the rock specimens. It is very difficult for water to move inside isolated pores. Thus, isolated pores were less influenced by freeze–thaw weathering.

Visualized images of equivalent diameter and local thickness show clear existence of parallel lamination inside the rock specimens. Tables 2 and 3 show that larger diameters relate to greater variation. The freezing point depression was affected by the diameter of pores (Camuffo 2014; De Kock et al. 2015) such that

$$T_f = -273 \frac{2\sigma}{r\rho L} \tag{4}$$

where r is the radius of a spherical ice crystal, ρ is ice density, and L is the latent heat of fusion. The equation means that smaller pores relate to greater freezing point depression. Theoretically, the freezing point can be low, at about $-40\text{ }^\circ\text{C}$, which is the self-nucleation temperature (Fagerland 1973). Thus, the water inside small pores can exist as supercooled water rather than ice crystals. The water inside pores larger than $20\text{ }\mu\text{m}$ is rarely influenced by freezing point depression. In addition, supercooled water inside small pores can migrate to large ice crystals that previously formed inside large pores. We postulate the increase in equivalent diameter from 0 to $50\text{ }\mu\text{m}$ can be attributed to newly formed pores or the expansion of pores to sizes larger than the detection limit of micro-CT.

The analysis of crack orientation showed that although major orientation remained as weathering progressed, the anisotropy of the orientations weakened. The main orientation was the same as the orientation of the thin parallel lamination in the specimens. Interestingly, the rate of change in orientation was greater (lower) at the lowest (highest) orientation direction. That is, microcracks developed vertical to the existing lamination.

Two models of frost weathering were used: volumetric expansion and ice segregation (Walder and Hallet 1986).

Volumetric expansion occurs when the temperature decreases below the freezing temperature of water. Under ideal conditions at $-22\text{ }^\circ\text{C}$, ice pressure in a closed system can theoretically reach 207 MPa (Bland and Rolls 1998). The actual pressure exerted by ice crystal is much less than 207 MPa because it is difficult for water to be contained in a closed system without air bubbles (French 2007). The pressure can reach to 10–100 MPa in natural rocks, which is higher than the general tensile strength of rocks (Davidson and Nye 1985).

In the ice segregation model, frost weathering is caused by the growth of ice crystals in porous rocks. The ice accumulates by water migration to the ice crystals. Thus, cracks grow steadily and can occur in low-saturation conditions. In actual conditions, the ice segregation model is more effective than the volumetric expansion model because the degree of saturation should exceed of 91% in the latter model. In the case of the tracksite in Seoyu-ri, however, a sufficient amount of water flowed in. According to unmanned aerial vehicle images, 23.5% of the upper plane surface area was affected by groundwater. Thus, volumetric expansion as well as ice segregation is sufficiently influenced by frost weathering at the tracksite in the winter season.

Ice segregation also can influence bedrock and the rock surface at the site. The research of Murton et al. (2001) shows that the upper part of a chalk specimen can be brecciated by ice segregation action under a temperature range of -0.2 to $-2.5\text{ }^\circ\text{C}$. Frost heaving and settlement were also noted in their study. These phenomena would be fatal for the conservation of dinosaur footprints.

One hundred cycles of laboratory tests correspond to frost weathering at the site during 18 months. However, the following differences were noted between weathering under actual conditions and those under laboratory testing:

1. The temperature variation and gradient in the laboratory experiment were exaggerated. The average annual

Table 3 Changes on the number of pores of HS-2 in each equivalent diameter group

Equivalent diameter	Frequency			Rate of change (%)
	Initial state	50 cycles	100 cycles	
0–50	31,040	31,810	35,104	+13
50–100	5445	5721	5904	+8
100–150	569	627	636	+12
150–200	201	215	207	+3
200–250	145	136	161	+11
250–300	80	91	83	+4
300–350	62	63	63	+2
350–400	26	35	39	+50
>400	25	32	34	+36
Total	37,593	38,730	42,231	12

minimum and maximum temperatures were used as the temperature variation range. Although the temperature gradient was set as 0.8 °C/min to minimize the effects of thermal shocking, unexpected thermal shocking can occur during testing. In addition, solar radiation affected the temperature variation. Thus, it is inferred that thermal shock is greater under actual conditions. Ice segregation is more effective when the ice crystals grow steadily. In this experiment, however, temperatures varied more frequently, resembling diurnal variation; therefore, the effect by volumetric expansion was greater.

2. The degree of saturation also affected the results. According to Matsuoka (Masuoka 1990), frost weathering occurs at 50% saturation and is significant when the value exceeds 92%. Because the rock specimens were completely saturated and water was supplied continuously in this study, the frost weathering was exaggerated.
3. This experiment represented a special case of saturated rock cooled from every direction; such a case is rare under natural conditions. In this case, the volumetric expansion model is more important.
4. Although the rock mass contained abundant discontinuities, few were included in the intact rock. Thus, the frost weathering effect tends to be underestimated because most water is located in the discontinuities.
5. Chemical and biological weathering are both important at the site. In this study, however, we focused on physical weathering by frost action.

The necessity of laboratory frost weathering has been questioned by some researchers owing to the gap between field surveys and laboratory experiments (Wiman 1963). However, artificial frost weathering experiments are meaningful for the following reasons. It is very difficult to acquiring accurate information about a rock mass. Although indirect information can be obtained by using some methods such as geophysical investigation, it is difficult to compare variations in the properties before and after frost weathering. In laboratory experiments, physical, chemical, and microstructural properties can be measured and monitored continuously with high accuracy. Moreover, frost weathering conditions such as temperature, humidity, and degree of saturation can also be controlled.

Conclusions

Experimental frost weathering simulating the geological and meteorological conditions of the dinosaur tracksite of Seoyu-ri, Hwasun, Korea, was performed in this study with up to 100 freeze–thaw cycles. Because every measurement

was performed by using non-destructive methods, the variation in same specimens can be analyzed continuously. In particular, three-dimensional quantitative analysis inside rock specimens was performed by using the micro-CT method. The methodology used in the study can be applied to other research investigating changes in the same specimens.

The tracksite has high geological and cultural value; therefore, its preservation is crucial. Frost weathering can cause disintegration of rock, which can destroy cultural heritage sites. After assessing the influence of frost weathering on the tracksite, this research suggests the construction of a shelter to maintain the temperature of the tracksite and to repair the drainage to prevent groundwater seepage. These treatments also can protect the site from temperature changes owing to solar radiation.

This research can be applied to assess the effects of frost weathering in other cultural stone heritage or geological heritage sites, particularly those consisting of sedimentary rocks. The results can also be used to evaluate the deterioration of rock in cold regions and to investigate the decay process in cold storage caverns.

Acknowledgements This work was supported by the National Research Foundation of Korea (NRF) grant funded by the Korea government (MEST; no. 2011-0027520).

References

- Altindag R, Alyildiz IS, Onargan T (2004) Mechanical property degradation of ignimbrite subjected to recurrent freeze–thaw cycles. *Int J Rock Mech Min* 41:1023–1028. doi:10.1016/j.ijrmms.2004.03.005
- Bland W, Rolls D (1998) *Weathering: An introduction to the scientific principles*. Arnold, London
- Brown ET (1981) *Rock characterization testing & monitoring*. Pergamon Press, Oxford
- Camuffo D (2014) *Microclimate for cultural heritage*. Elsevier, Oxford
- Davidson GP, Nye JF (1985) A photoelastic study of ice pressure in rock cracks. *Cold Reg Sci Technol* 11:141–153. doi:10.1016/0165-232X(85)90013-8
- De Kock T, Boone MA, De Schryver T, Van Stappen J, Derluyn H, Masschaele B, De Schutter G, Cnudde V (2015) A pore-scale study of fracture dynamics in rock using X-ray micro-CT under ambient freeze–thaw cycling. *Environ Sci Technol* 49:2867–2874. doi:10.1021/es505738d
- Delerue JF, Perrier E, Yu ZY, Velde B (1999) New algorithms in 3D image analysis and their application to the measurement of a spatialized pore size distribution in soils. *Phys Chem Earth Pt A* 24:639–644
- Fagerland G (1973) Determination of pore-size distribution from freezing-point depression. *Matér et Constr* 6:215–225
- French HM (2007) *The periglacial environment*. Wiley, West Sussex
- Grassegger G (1999) Decay mechanisms of natural building stones on monuments: A review of the latest theories. In: Stumpp S, Krüger M, Große C (ed) *Werkstoffe und Werkstoffprüfung im*

- Bauwesen. Institut für Werkstoffe im Bauwesen, Universität Stuttgart, Stuttgart, pp 54–81
- Hall K (1999) The role of thermal stress fatigue in the breakdown of rock in cold regions. *Geomorphology* 31:47–63
- Houck KJ, Lockley MG (2006) Life in an active volcanic arc: petrology and sedimentology of dinosaur track beds in the Jindong Formation (Cretaceous), Gyeongsang Basin, South Korea. *Cretac Res* 27:102–122. doi:10.1016/j.cretres.2005.10.004
- Huh M, Paik IS, Lockley MG, Hwang KG, Kim BS, Kwak SK (2006) Well-preserved theropod tracks from the Upper Cretaceous of Hwasun County, southwestern South Korea, and their paleobiological implications. *Cretac Res* 27:123–138. doi:10.1016/j.cretres.2005.10.003
- Kim BS, Huh M (2010) Analysis of the acceleration phase of a theropod dinosaur based on a Cretaceous trackway from Korea. *Palaeogeogr Palaeoclimatol* 293:1–8. doi:10.1016/j.palaeo.2010.04.020
- Kim JY, Lockley MG (2012) New sauropod tracks (*Brontopodus pentadactylus* ichnosp. nov.) from the early cretaceous haman formation of Jinju Area, Korea: implications for sauropods manus morphology. *Ichnos* 19:84–92. doi:10.1080/10420940.2012.664056
- Kim BK, Park BK (1966) The geological map of Dongbok sheet (1:50,000). Geological Survey of Korea, Seoul (in Korean)
- Lee SK, Park HD (2014) Comparison of observation and laboratory slaking tests in the assessment of coastal erosion in Cheju Island, Korea. *Geosyst Eng* 17:136–141. doi:10.1080/12269328.2014.931258
- Lockley MG, Huh M, Kim BS (2012) Ornithomimid tracks and pes-only sauropod trackways from the hwasun tracksite, cretaceous of Korea. *Ichnos* 19:93–100. doi:10.1080/10420940.2011.625726
- Martínez-Martínez J, Benavente D, Gomez-Heras M, Marco-Castaño L, García-del-Cura MÁ (2013) Non-linear decay of building stones during freeze–thaw weathering processes. *Constr Build Mater* 38:443–454. doi:10.1016/j.conbuildmat.2012.07.059
- Masuoka N (1990) Mechanisms of rock breakdown by frost action: an experimental approach. *Cold Reg Sci Technol* 17:253–270
- Minter NJ, Lockley MG, Huh M, Hwang KG, Kim JY (2012) Lithographus, an abundant arthropod trackway from the cretaceous haenam tracksite of Korea. *Ichnos* 19:115–120. doi:10.1080/10420940.2011.625756
- Murton JB, Coutard JP, Lautridou JP, Ozouf JC, Robinson DA, Williams RBG (2001) Physical modelling of bedrock brecciation by ice segregation in permafrost. *Permafrost Periglacial* 12:255–266. doi:10.1002/ppp.390
- Nicholson DT, Nicholson FH (2000) Physical deterioration of sedimentary rocks subjected to experimental freeze–thaw weathering. *Earth Surf Process Landf* 25:1295–1307. doi:10.1002/1096-9837(200011)25:12<1295:AID-ESP138>3.0.CO;2-E
- Paik IS, Huh M, Park KH, Hwang KG, Kim KS, Kim HJ (2006) Yeosu dinosaur track sites of Korea: the youngest dinosaur track records in Asia. *J Asian Earth Sci* 28:457–468. doi:10.1016/j.jseaes.2005.11.007
- Park J, Hyun CU, Park HD (2015) Changes in microstructure and physical properties of rocks caused by artificial freeze–thaw action. *Bull Eng Geol Environ* 74:555–565. doi:10.1007/s10064-014-0630-8
- Potts AS (1970) Frost action in rocks: some experimental data. *T I Brit Geogr* 49:109–124
- Prick A (1997) Critical degree of saturation as a threshold moisture level in frost weathering of limestones. *Permafrost Periglacial* 8:91–99. doi:10.1002/(SICI)1099-530(199701)8:1<91:AID-PPP238>3.0.CO;2-4
- Ruiz de Argandoña VG, Rodríguez Rey A, Celorio C, Suárez del Río LM, Calleja L, Llavona J (1999) Characterization by computed X-ray tomography of the evolution of the pore structure of a dolomite rock during freeze–thaw cyclic tests. *Phys Chem Earth Pt A* 24:633–637
- Saliu M, Lawal AI (2014) Investigations of weathering effects on engineering properties of Supare granite gneiss. *J Min World Express* 3:53–62. doi:10.14355/mwe.2014.03.008
- Shang Y, Yue Z, Park HD, Hyun CU (2015) Brittle fracture and plastic creep of the completely decomposed granite presented in CT. *Geosyst Eng* 18:338–347. doi:10.1080/12269328.2015.1075438
- Shen B, Jung YB, Park ES, Kim TK (2015) Modelling the effect of ice swelling in the rock mass around an LNG underground storage cavern using FRACOD. *Geosyst Eng* 18:181–198. doi:10.1080/12269328.2015.1044575
- Thomachot C, Matsuoka N (2007) Dilation of building materials submitted to frost action. In: Prikryl R, Smith BJ (eds) *Building stone decay: from diagnosis to conservation*. Geol Soc, London, pp 167–177
- Tugrul A, Zarif IH (2000) The influence of weathering on the geological and geomechanical characteristics of a sandstone in Istanbul, Turkey. *Environ Eng Geosci* 6:403–412. doi:10.2113/gsegeosci.6.4.403
- Walder JS, Hallet B (1986) The physical basis of frost weathering: toward a more fundamental and unified perspective. *Arctic Alp Res* 18:27–32
- Wiman S (1963) A Preliminary study of experimental frost weathering. *Geogr Ann* 45:113–121. doi:10.2307/520387
- Yang SY (1982) On the dinosaur's footprints from the upper cretaceous gyeongsang group, Korea. *J Geol Soc Korea* 18:37–48 (in Korean with English abstract)